

Electroweak Radiative Corrections to Single-top Production.

D. Bardin¹ e-mail: bardin@nusun.jinr.ru, S. Bondarenko², L. Kalinovskaya¹, V. Kolesnikov¹, and W. von Schlippe³

¹ Dzhelepov Laboratory for Nuclear Problems, JINR,
JINR, Dubna, 141980 Russia

² Bogoliubov Laboratory of Theoretical Physics, JINR,
JINR, Dubna, 141980 Russia

³ Petersburg Nuclear Physics Institute, Gatchina, 188300 Russia

Received: date / Revised version: date

Abstract. Radiative corrections to the single top s and t channel production processes are revisited. Complete one-loop electroweak corrections are calculated within the **SANC** system. New is a study of the regularisation of the top-legs associated infrared divergences with aid of the complex mass of the top quark. A comparison of these electroweak corrections with those computed by the conventional method is presented both for top production and decays. Standard FORM and FORTRAN **SANC** modules are created. These modules are compiled into a package **sanc_cc_v1.40**, which may be downloaded from **SANC** project homepages. Numerous numerical results are presented at the partonic level with the aim to demonstrate the correct working of modules. These modules are intended to be used in Monte Carlo generators for single top production at the LHC. Where possible, we compare our results with those existing in the literature; in particular, a comprehensive comparison with results of the **CompHEP** system is given.

Key words. electroweak radiative corrections – helicity amplitudes

PACS. 1 2.15.-y Electroweak interactions; 12.15.Lk Electroweak radiative corrections

1 Introduction

In continuation of work on electroweak one-loop corrections to processes involving the top quark [1, 2], we present here a calculation of EW one-loop corrections to single top quark production and top quark decay. To incorporate these processes in the **SANC** framework [3] is a natural extension of the previous work.

The interest in the study of single top production has been stated many times (see *e.g.* [4] and references therein), suffice it to say that this is the only way of measuring the CKM matrix element $|V_{tb}|$ directly and thereby providing a sensitive test of the 3-generation scheme of the Standard Model. Indeed, a significant deviation of $|V_{tb}|$ from the value demanded by unitarity of the CKM matrix would be an indication of the presence of a fourth generation of fundamental fermions.

Precision calculations of single top quark production have been done for a number of years (see *e.g.* [5] and references therein) but remain of continued interest. This is motivated on the one hand by the observation of such events at the Tevatron D0 [6, 7] and CDF [8, 9] and, on the other hand, by the need to prepare software to analyse single top quark events at the LHC, running at 7 TeV.

Most of the theoretical work in single top production has been concerned with higher order QCD corrections, leading to the development of Monte Carlo

generators, such as MC@NLO [10] or SingleTop [11], incorporated in the standard LHC tools.

There are three channels of single top quark production: t channel, s channel and associated production. The t channel process, $bq \rightarrow tq'$, where q and q' are light quarks, is the channel known to have the largest cross section [12–15]. Calculations for the LHC at 14 TeV have led to the prediction of this cross section being more than an order of magnitude greater than that of the s channel process $qq' \rightarrow tb$ and about four times greater than the cross section of associated production $qg \rightarrow tW$ (see *e.g.* [16]), and it has been stated that the electroweak corrections are of comparable magnitude to the QCD corrections [12].

In this paper we calculate the electroweak corrections to the s and t channels of single top quark production and revisit the top quark decay [2]. The important new feature of the present work is the inclusion in the calculations of the width Γ_t of the top quark. This is a nontrivial step, and we will show that the results are sensitive to Γ_t .

The paper is organized as follows.

In section 2 we present the covariant amplitudes for the processes under consideration, working within the framework of the *multichannel approach* (see Ref [17]). In section 3 we introduce the infrared regularisation by the complex mass of the top quark, at first for the virtual QED corrections, and then for the hard photon

radiation. Numerical results are presented in section 4 and the Conclusions and Outlook in section 5.

2 Covariant Amplitude

In this section we proceed in the spirit of “multi-channel approach”, see Ref. [17]. First, we consider annihilation into vacuum with all particles incoming.

2.1 All particles incoming

It is convenient to consider two vacuum diagrams:

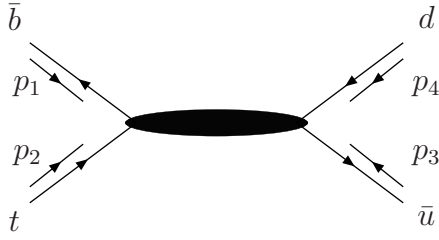


Fig. 1. The $t\bar{b}u\bar{d} \rightarrow 0$ processes

and

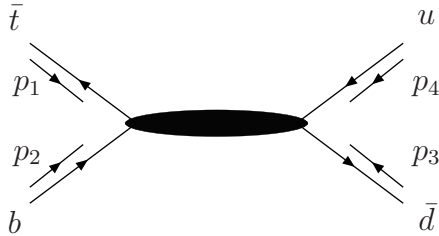


Fig. 2. The $t\bar{b}u\bar{d} \rightarrow 0$ processes

Here black ovals symbolically denote all one-loop insertions to the corresponding tree diagrams.

Covariant Amplitudes (CA) of Figs. 1 and 2 are characterized by four different structures and scalar Form Factors (FF) if the mass of the light quarks is neglected and b quark mass is not neglected. Omitting Dirac spinors, one may write a common expression for this CA of the process in terms of scalar form factors, $\mathcal{F}_{LL}(s, t)$, see [3]:

$$\begin{aligned} \mathcal{A} = i e^2 \frac{d_w(s)}{4} & \left[\gamma_\mu (1 + \gamma_5) \otimes \gamma_\mu (1 + \gamma_5) \mathcal{F}_{LL}(s, t) \right. \\ & + \gamma_\mu (1 - \gamma_5) \otimes \gamma_\mu (1 + \gamma_5) \mathcal{F}_{RL}(s, t) \\ & + (1 + \gamma_5) \otimes \gamma_\mu (1 + \gamma_5) (-i D_\mu) \mathcal{F}_{LD}(s, t) \\ & \left. + (1 - \gamma_5) \otimes \gamma_\mu (1 + \gamma_5) (-i D_\mu) \mathcal{F}_{RD}(s, t) \right], \quad (1) \end{aligned}$$

with

$$D_\mu = (p_1 - p_2)_\mu, \quad (2)$$

and 4-momentum conservation reads

$$p_1 + p_2 + p_3 + p_4 = 0, \quad (3)$$

the invariants are defined by

$$s = -(p_1 + p_2)^2, \quad t = -(p_2 + p_3)^2, \quad (4)$$

and

$$d_w(s) = \frac{V}{2s_W^2} \frac{1}{s - M_W^2 + iM_W\Gamma_W}. \quad (5)$$

Here $V = V_{tb}V_{ud}$ is the relevant product of CKM matrix elements and the symbol \otimes means, considering the factor of \mathcal{F}_{LL} in diagram Fig. 1,

$$\gamma_\mu \gamma_+ \otimes \gamma_\mu \gamma_+ = \bar{u}(p_2) \gamma_\mu \gamma_+ v(p_1) \bar{v}(p_3) \gamma_\mu \gamma_+ u(p_4)$$

$$\text{with} \quad \gamma_+ = 1 + \gamma_5$$

and appropriate changes in the other cases. The scalar form factors \mathcal{F} are labeled according to their structures, see [3].

2.2 Conversion to top decay

The CA for the decay $t(p_2) \rightarrow b(p_1) + u(p_3) + \bar{d}(p_4)$ is derived from Fig. 1 by the following 4-momentum replacement:

$$\begin{aligned} p_1 &\rightarrow -p_1, & p_3 &\rightarrow -p_3, \\ p_2 &\rightarrow p_2, & p_4 &\rightarrow -p_4. \end{aligned}$$

For the decay $\bar{t}(p_1) \rightarrow \bar{b}(p_2) + d(p_3) + \bar{u}(p_4)$ it is more transparent to make the replacement from Fig. 2:

$$\begin{aligned} p_1 &\rightarrow p_1, & p_3 &\rightarrow -p_3, \\ p_2 &\rightarrow -p_2, & p_4 &\rightarrow -p_4. \end{aligned}$$

As a result one has two decay diagrams, schematically representing one-loop EW corrections:

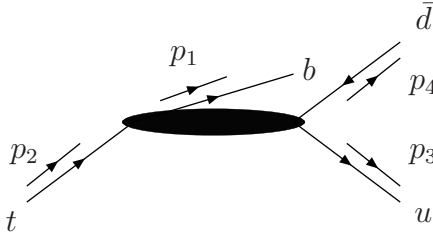


Fig. 3. The $t \rightarrow bud\bar{}$ processes

From the diagram of Fig. 3 the four Helicity Amplitudes (HA) can be derived by the standard techniques used in **SANC**, see Eqs. (47-50) of Ref. [3].

For the case of the process of diagram of Fig. 4 the HA are similar, although not identical. For their exact expressions see the relevant module in the **SANC** tree.

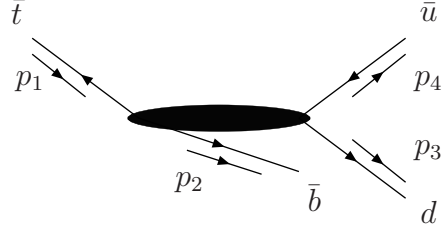


Fig. 4. The $\bar{t} \rightarrow \bar{b}ud$ processes

2.3 Conversion to s channel

The CA for the s channel single-top production processes $\bar{u}(p_1) + d(p_2) \rightarrow b(p_3) + \bar{t}(p_4)$ is obtained from Fig. 1 by the following 4-momentum replacement:

$$\begin{aligned} p_1 &\rightarrow -p_3, & p_3 &\rightarrow p_1, \\ p_2 &\rightarrow -p_4, & p_4 &\rightarrow p_2, \end{aligned}$$

leading to the diagram

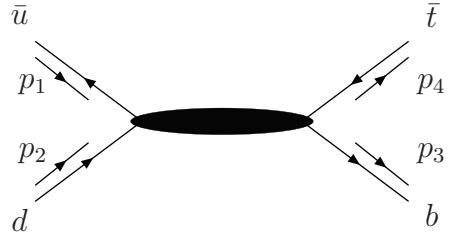


Fig. 5. The $\bar{u}d \rightarrow \bar{t}b$ process

For the processes $\bar{d}(p_1) + u(p_2) \rightarrow t(p_3) + \bar{b}(p_4)$ from Fig. 2 the conversion

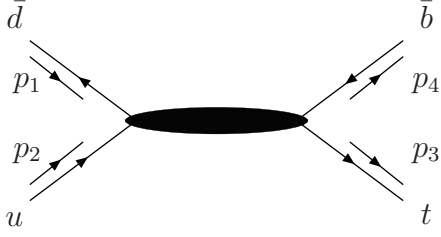
$$\begin{aligned} p_1 &\rightarrow -p_3, & p_3 &\rightarrow p_1, \\ p_2 &\rightarrow -p_4, & p_4 &\rightarrow p_2, \end{aligned}$$

leads to the diagram of Fig. 6.

For the corresponding HA one can get rather compact expressions.

- Helicity amplitude for $\bar{u}d \rightarrow \bar{t}b$

$$\mathcal{H}_{+---} = k_0 \sin \vartheta \{ (m_t k_1 + m_b k_2) \mathcal{F}_{LL}$$

**Fig. 6.** The $\bar{d}u \rightarrow \bar{t}b$ processes

$$\begin{aligned}
& +(m_t k_2 + m_b k_1) \mathcal{F}_{LR} \\
& -P^+ P^- (k_2 \mathcal{F}_{LD} - k_1 \mathcal{F}_{RD}) \}, \\
\mathcal{H}_{+--+} &= k_0 \sin \vartheta \{ (m_t k_2 + m_b k_1) \mathcal{F}_{LL} \\
& +(m_t k_1 + m_b k_2) \mathcal{F}_{LR} \\
& +P^+ P^- (k_1 \mathcal{F}_{LD} - k_2 \mathcal{F}_{RD}) \}, \\
\mathcal{H}_{+---} &= k_0 \sqrt{s} c_+ (k_1 \mathcal{F}_{LL} + k_2 \mathcal{F}_{LR}), \\
\mathcal{H}_{+--+} &= k_0 \sqrt{s} c_- (k_2 \mathcal{F}_{LL} + k_1 \mathcal{F}_{LR}). \quad (6)
\end{aligned}$$

• Helicity amplitude for $\bar{d}u \rightarrow \bar{t}b$

$$\begin{aligned}
\mathcal{H}_{+---} &= k_0 \sin \vartheta \{ (m_t k_2 + m_b k_1) \mathcal{F}_{LL} \\
& +(m_t k_1 + m_b k_2) \mathcal{F}_{LR} \\
& -P^+ P^- (k_2 \mathcal{F}_{LD} - k_1 \mathcal{F}_{RD}) \}, \\
\mathcal{H}_{+--+} &= k_0 \sin \vartheta \{ (m_t k_1 + m_b k_2) \mathcal{F}_{LL} \\
& +(m_t k_2 + m_b k_1) \mathcal{F}_{LR} \\
& +P^+ P^- (k_1 \mathcal{F}_{LD} - k_2 \mathcal{F}_{RD}) \}, \\
\mathcal{H}_{+--+} &= k_0 \sqrt{s} c_- (k_2 \mathcal{F}_{LL} + k_1 \mathcal{F}_{LR}), \\
\mathcal{H}_{+---} &= k_0 \sqrt{s} c_+ (k_1 \mathcal{F}_{LL} + k_2 \mathcal{F}_{LR}). \quad (7)
\end{aligned}$$

Here

$$\begin{aligned}
k_0 &= -\frac{1}{2} V \chi(M_W^2, s), \\
\chi(M_W^2, s) &= \frac{s}{2s_W^2} \frac{1}{s - M_W^2 + iM_W \gamma_W}
\end{aligned}$$

$$k_{1,2} = P^- \pm P^+,$$

$$P^\pm \equiv \sqrt{s - (m_t \pm m_b)^2},$$

$$c_\pm = 1 \pm \cos \vartheta \quad (8)$$

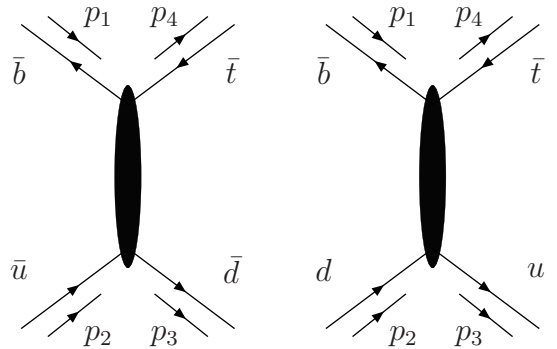
and ϑ is always the angle $\angle(\mathbf{p}_1, \mathbf{p}_3)$.

2.4 Conversion to t channel processes

In the CAs for the t channel single-top production processes $\bar{b}(p_1) + \bar{u}(p_2) \rightarrow \bar{d}(p_3) + \bar{t}(p_4)$ and $\bar{b}(p_1) + d(p_2) \rightarrow u(p_3) + \bar{t}(p_4)$ it is convenient to make the replacement “in pairs”. From Fig. 1 one may perform two 4-momentum replacements:

$$\begin{aligned}
p_1 &\rightarrow p_1, & p_1 &\rightarrow p_1, \\
p_2 &\rightarrow -p_4, & p_2 &\rightarrow -p_4, \\
p_3 &\rightarrow p_2, & p_3 &\rightarrow -p_3, \\
p_4 &\rightarrow -p_3, & p_4 &\rightarrow p_2,
\end{aligned}$$

which give rise to two different physical t channel processes, described by two symbolic diagrams:

**Fig. 7.** The $\bar{b}\bar{u} \rightarrow \bar{t}\bar{d}$ and $\bar{b}d \rightarrow \bar{t}u$ processes

For the processes $b(p_1) + u(p_2) \rightarrow t(p_4) + d(p_3)$ and $b(p_1) + \bar{d}(p_2) \rightarrow t(p_4) + \bar{u}(p_3)$, the pair of replacements

from Fig. 2,

$$\begin{array}{ll} p_1 \rightarrow -p_4, & p_1 \rightarrow -p_4, \\ p_2 \rightarrow p_1, & p_2 \rightarrow p_1, \\ p_3 \rightarrow -p_3, & p_3 \rightarrow p_2, \\ p_4 \rightarrow p_2, & p_4 \rightarrow -p_3, \end{array}$$

gives the corresponding pair of symbolic diagrams for the two remaining t channel processes:

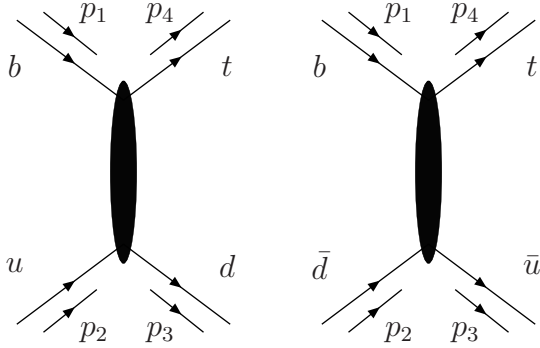


Fig. 8. The $bu \rightarrow td$ and $b\bar{d} \rightarrow t\bar{u}$ processes

The HAs are all different for the four types of processes. They are listed below in another sequence than they were presented diagrammatically above. First, we give the more complicated HAs for 4-particle and 4-antiparticle processes:

- Helicity amplitudes for $ub \rightarrow td$

$$\begin{aligned} \mathcal{H}_{----} = & k_0 \left\{ N^+ \sqrt{s} c_+ \left[2m_{t+b} \mathcal{F}_{LL} \right. \right. \\ & \left. \left. + \frac{m_t}{s} (c_- s_b \mathcal{F}_{RL} - k_2 \mathcal{F}_{LD}) - k_1 \mathcal{F}_{RD} \right] \right. \\ & \left. - N^- c_- \left[2s_{tb} \mathcal{F}_{LL} \right. \right. \\ & \left. \left. - m_t \left(\frac{k_2}{s} \mathcal{F}_{RL} + c_+ s_b (\mathcal{F}_{LD} - \mathcal{F}_{RD}) \right) \right] \right\}, \end{aligned}$$

$$\begin{aligned} \mathcal{H}_{----+} = & k_0 \sin \vartheta \left\{ N^+ c_+ s_b \left[\mathcal{F}_{RL} \right. \right. \\ & \left. \left. + m_t (\mathcal{F}_{LD} - \mathcal{F}_{RD}) \right] \right\} \end{aligned}$$

$$\begin{aligned} & + N^- \sqrt{s} \left[\frac{k_2}{s} \mathcal{F}_{RL} \right. \\ & \left. - k_1 \mathcal{F}_{LD} - \frac{m_t k_2}{s} \mathcal{F}_{RD} \right] \Big\}, \end{aligned}$$

$$\begin{aligned} \mathcal{H}_{+---} = & k_0 \sin \vartheta \left\{ -N^+ \left[2s_{tb} \mathcal{F}_{LL} \right. \right. \\ & \left. \left. - m_t \left(\frac{k_2}{s} \mathcal{F}_{RL} + c_+ s_b (\mathcal{F}_{LD} - \mathcal{F}_{RD}) \right) \right] \right. \\ & \left. - N^- \sqrt{s} \left[2m_{t+b} \mathcal{F}_{LL} \right. \right. \\ & \left. \left. + \frac{m_t}{s} (c_- s_b \mathcal{F}_{RL} - k_2 \mathcal{F}_{LD}) - k_1 \mathcal{F}_{RD} \right] \right\}, \end{aligned}$$

$$\begin{aligned} \mathcal{H}_{+--+} = & k_0 c_+ \left\{ N^+ \sqrt{s} \left(\frac{k_2}{s} \mathcal{F}_{RL} \right. \right. \\ & \left. \left. - k_1 \mathcal{F}_{LD} - \frac{m_t k_2}{s} \mathcal{F}_{RD} \right) \right. \\ & \left. - N^- c_- s_b [\mathcal{F}_{RL} + m_t (\mathcal{F}_{LD} - \mathcal{F}_{RD})] \right\}. \end{aligned} \quad (9)$$

Specific to Eq. (9) is the following notation:

$$\begin{aligned} k_0 &= V \chi(M_W^2, s) N^2 N_{(2,3)}^-, \\ k_1 &= 2s_{tb} - c_+ s_b, \\ k_2 &= 2s_{tb} m_b + c_+ m_t s_b. \end{aligned} \quad (10)$$

The other notation common to Eqs. (9) and (13) is

$$\begin{aligned} s_{tb} &= s + m_t m_b, & m_{t+b} &= m_t + m_b, \\ s_t &= s - m_t^2, & s_b &= s - m_b^2, \\ c_{\pm} &= 1 \pm \cos \vartheta, \end{aligned} \quad (11)$$

and

$$\begin{aligned} N &= \sqrt{\frac{2s}{s_{tb}^2 c_- + s m_t^2 c_+}}, \\ N_{(2,3)}^- &\equiv N_{(3,2)}^- = \sqrt{\frac{s_t s_b}{2}}, \\ N^+ &= \frac{m_{t+b}}{\sqrt{2}}, \quad N^- = \frac{s_{tb}}{\sqrt{2s}}. \end{aligned} \quad (12)$$

- Helicity amplitudes for $\bar{b}\bar{u} \rightarrow \bar{t}\bar{d}$

$$\mathcal{H}_{----} = k_0 \left\{ -N^+ \sqrt{s} c_+ \left[\frac{k_2}{s} \mathcal{F}_{RL} \right. \right.$$

$$\begin{aligned}
& - (2m_{t+b}m_t + c_-s_t)\mathcal{F}_{LD} - \frac{m_b k_2}{s}\mathcal{F}_{RD} \Big] \\
& - N^- c_- \Big[2s_{tb}\mathcal{F}_{LL} \\
& - m_b \Big(\frac{k_2}{s}\mathcal{F}_{RL} + c_+s_t(\mathcal{F}_{LD} - \mathcal{F}_{RD}) \Big) \Big] \Big\}, \\
\mathcal{H}_{----+} &= k_0 \sin \vartheta \Big\{ N^+ \Big[2s_{tb}\mathcal{F}_{LL} \\
& - m_b \Big(\frac{k_2}{s}\mathcal{F}_{RL} + c_+s_t(\mathcal{F}_{LD} - \mathcal{F}_{RD}) \Big) \Big] \\
& - N^- \sqrt{s} \Big[\frac{k_2}{s}\mathcal{F}_{RL} \\
& - k_1\mathcal{F}_{LD} - \frac{m_b k_2}{s}\mathcal{F}_{RD} \Big] \Big\}, \\
\mathcal{H}_{+---} &= k_0 \sin \vartheta \Big\{ -N^+ c_+ s_t [\mathcal{F}_{RL} \\
& + m_b (\mathcal{F}_{LD} - \mathcal{F}_{RD})] \\
& + N^- \sqrt{s} \Big[2m_{t+b}\mathcal{F}_{LL} \\
& + \frac{m_b}{s} (c_-s_t\mathcal{F}_{RL} - k_2\mathcal{F}_{LD}) - k_1\mathcal{F}_{RD} \Big] \Big\}, \\
\mathcal{H}_{+--+} &= k_0 c_+ \Big\{ -N^+ \sqrt{s} \Big[2m_{t+b}\mathcal{F}_{LL} \\
& + \frac{m_b}{s} (c_-s_t\mathcal{F}_{RL} + k_2\mathcal{F}_{LD}) + k_1\mathcal{F}_{RD} \Big] \\
& - N^- c_- s_t [\mathcal{F}_{RL} + m_b (\mathcal{F}_{LD} - \mathcal{F}_{RD})] \Big\} \quad (13)
\end{aligned}$$

$$\begin{aligned}
\mathcal{H}_{+++-} &= k_0 \sqrt{s} \sin \vartheta \left[\frac{m_b}{s} (\mathcal{F}_{LL} - m_t \mathcal{F}_{LD}) - \mathcal{F}_{RD} \right], \\
\mathcal{H}_{++++} &= -k_0 \left[\frac{m_t m_b c_-}{s} \mathcal{F}_{LL} - 2\mathcal{F}_{RL} \right. \\
& \left. + c_+ (m_b \mathcal{F}_{LD} + m_t \mathcal{F}_{RD}) \right]. \quad (15)
\end{aligned}$$

• Helicity amplitudes for $\bar{b}d \rightarrow \bar{t}u$

$$\begin{aligned}
\mathcal{H}_{-----} &= -k_0 \left[\frac{m_t m_b c_-}{s} \mathcal{F}_{LL} - 2\mathcal{F}_{RL} \right. \\
& \left. + c_+ (m_t \mathcal{F}_{LD} + m_b \mathcal{F}_{RD}) \right], \\
\mathcal{H}_{----+} &= -k_0 \sqrt{s} \sin \vartheta \left(\frac{m_b}{s} \mathcal{F}_{LL} \right. \\
& \left. - \mathcal{F}_{LD} - \frac{m_t m_b}{s} \mathcal{F}_{RD} \right), \\
\mathcal{H}_{+----} &= k_0 \sqrt{s} \sin \vartheta \\
& \times \left[\frac{m_t}{s} (\mathcal{F}_{LL} - m_b \mathcal{F}_{LD}) - \mathcal{F}_{RD} \right], \\
\mathcal{H}_{+--+} &= k_0 c_+ (\mathcal{F}_{LL} - m_b \mathcal{F}_{LD} - m_t \mathcal{F}_{RD}). \quad (16)
\end{aligned}$$

In Eqs. (15) and (16)

$$k_0 = V\chi(M_w^2, s)P^+(s, 0, m_b)P^+(s, 0, m_t), \quad (17)$$

Notation specific to Eq. (13) is:

$$\begin{aligned}
k_0 &= V\chi(M_w^2, s)N^2 N_{(3,2)}^-, \\
k_1 &= 2s_{tb} - c_+s_t, \\
k_2 &= 2s_{tb}m_t + c_+m_b s_t. \quad (14)
\end{aligned}$$

Next we give HAs for the t channel process of annihilation of different flavors; they are simpler than the previous ones.

- Helicity amplitudes for $b\bar{d} \rightarrow t\bar{u}$

$$\begin{aligned}
\mathcal{H}_{-++-} &= k_0 c_+ (\mathcal{F}_{LL} - m_t \mathcal{F}_{LD} - m_b \mathcal{F}_{RD}), \\
\mathcal{H}_{-+++} &= -k_0 \sqrt{s} \sin \vartheta \left(\frac{m_t}{s} \mathcal{F}_{LL} \right. \\
& \left. - \mathcal{F}_{LD} - \frac{m_t m_b}{s} \mathcal{F}_{RD} \right),
\end{aligned}$$

with a function typical to helicity amplitudes:

$$P^\pm(s, x, y) = \sqrt{s - (x \pm y)^2}. \quad (18)$$

3 Infrared regularization by the complex top quark mass.

Infrared divergences associated with interactions of photons with on-mass-shell top legs in the limit of zero width of the top quark may be regularized by any conventional method (photon mass, dimensional

regularisation), but physically they are naturally regularized by the presence of the finite top quark width Γ_t . Here this approach will be exploited.

3.1 Top quark width and virtual QED correction

There are three diagrams contributing to virtual one-loop QED corrections involving the top quark: see Figs. 9, 10 and 11.

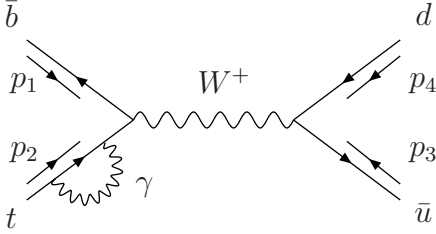


Fig. 9. The self-energy photonic QED correction for $t\bar{b}ud \rightarrow 0$ processes

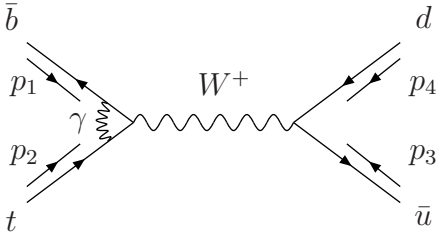


Fig. 10. The vertex photonic QED correction

The appropriate formalism was developed in Ref. [2]. In particular, it was shown that of the four scalar form factors \mathcal{F} only \mathcal{F}_{LL} contains IRD QED as well as weak contributions which can be separated thus:

$$\mathcal{F}_{LL} = 1 + \frac{e^2}{16\pi^2} \tilde{\mathcal{F}}_{LL}^{\text{QED}} + \frac{g^2}{16\pi^2} \tilde{\mathcal{F}}_{LL}^{\text{weak}} \quad (19)$$

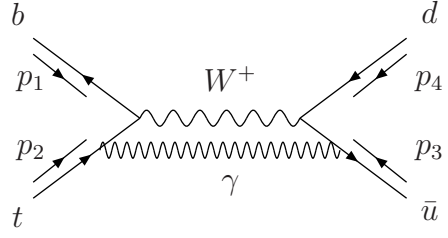


Fig. 11. The direct box photonic QED correction

and the expression for $\tilde{\mathcal{F}}_{LL}^{\text{QED}}$ was explicitly expressed in terms of standard Passarino–Veltman (PV) functions C_0 . To regulate the amplitude the photon was given a mass λ . However, one can alternatively introduce the top quark width, i.e. instead of

$$C_0(-m_t^2, -m_b^2, Q^2; m_t, \lambda, m_b)$$

we now write

$$C_0(-m_t^2, -m_b^2, Q^2; \tilde{m}_t, 0, m_b) \quad (20)$$

with $\tilde{m}_t^2 = m_t^2 + \Delta_t$, $\Delta_t = -im_t\Gamma_t$.

The corresponding replacement for the IRD term due to Fig. 9 reads

$$\ln\left(\frac{m_t^2}{\lambda^2}\right) \rightarrow -2\frac{\tilde{m}_t^2}{m_t^2} \ln\left(\frac{-im_t\Gamma_t}{\tilde{m}_t^2}\right). \quad (21)$$

The expression for the amplitude of Fig. 11 contains an infrared and mass singular D_0 function. In Ref. [18] we have shown that these functions can be reduced by standard Passarino–Veltman reduction to an infrared finite mass singular auxiliary function J_{AW}^d and a mass singular C_0 function. This has become standard SANC approach which we apply here.

The relevant C_0 function is

$$C_0^{\text{IR}} = C_0(-m_t^2, -m_b^2, Q^2; \tilde{m}_t, 0, m_b) \quad (22)$$

$$\begin{aligned}
&= \frac{1}{S_d} \left\{ \ln(y_{d1}) \ln\left(1 - \frac{1}{y_{d1}}\right) - \text{Li}_2\left(\frac{1}{y_{d1}}\right) \right. \\
&\quad - \text{Li}_2\left(\frac{1 - y_{d1}}{y_{d1} - y_{d1}}\right) + \text{Li}_2\left(-\frac{y_{d1}}{y_{d1} - y_{d1}}\right) \\
&\quad - \text{Li}_2\left(\frac{1 - y_{d1}}{y_{d2} - y_{d1}}\right) + \text{Li}_2\left(-\frac{y_{d1}}{y_{d2} - y_{d1}}\right) \\
&\quad - \ln(y_{d2}) \ln\left(1 - \frac{1}{y_{d2}}\right) + \text{Li}_2\left(\frac{1}{y_{d2}}\right) \\
&\quad + \text{Li}_2\left(\frac{1 - y_{d2}}{y_{d1} - y_{d2}}\right) - \text{Li}_2\left(-\frac{y_{d2}}{y_{d1} - y_{d2}}\right) \\
&\quad \left. + \text{Li}_2\left(\frac{1 - y_{d2}}{y_{d2} - y_{d2}}\right) - \text{Li}_2\left(-\frac{y_{d2}}{y_{d2} - y_{d2}}\right) \right\},
\end{aligned}$$

where

$$\begin{aligned}
B_d &= Q^2 + m_t^2 - m_b^2 + Q^2/|Q^2|i\varepsilon, \\
S_d &= \sqrt{(Q^2)^2 + 2Q^2(m_t^2 + m_b^2) + (m_t^2 - m_b^2)^2}, \\
y_{d1} &= \frac{B_d - S_d}{2Q^2}, \quad y_{d2} = \frac{B_d + S_d}{2Q^2}, \quad (23)
\end{aligned}$$

and

$$\begin{aligned}
B_l &= Q^2 + \tilde{m}_t^2 - m_b^2, \\
S_l &= \sqrt{(Q^2)^2 + 2Q^2(\tilde{m}_t^2 + m_b^2) + (\tilde{m}_t^2 - m_b^2)^2}, \\
y_{d1} &= \frac{B_l - S_l}{2Q^2}, \quad y_{d2} = \frac{B_l + S_l}{2Q^2}. \quad (24)
\end{aligned}$$

Its limit for $m_b \rightarrow 0$ is

$$\begin{aligned}
C_0^{\text{IR}} &= \frac{1}{B_d} \left\{ \ln\left(\frac{\Delta_t}{B_l}\right) \ln\left(\frac{m_b^2}{m_t^2}\right) - 2 \ln\left(\frac{B_d}{m_t^2}\right) \ln\left(\frac{\Delta_t}{m_t^2}\right) \right. \\
&\quad + \left[\frac{1}{2} \ln\left(\frac{B_d}{m_t^2}\right) + \ln\left(\frac{B_l}{m_t^2}\right) \right] \ln\left(\frac{B_d}{m_t^2}\right) \\
&\quad - \text{Li}_2\left(-\frac{\Delta_t}{m_t^2}\right) + \text{Li}_2\left(-\frac{\Delta_t}{B_d}\right) \\
&\quad \left. - \text{Li}_2\left(\frac{\Delta_t}{B_l}\right) - \text{Li}_2\left(\frac{Q^2}{B_l}\right) + \zeta(2) \right\}. \quad (25)
\end{aligned}$$

Here

$$\begin{aligned}
B_l &= Q^2 + \tilde{m}_t^2, \\
B_d &= Q^2 + m_t^2 - i\varepsilon. \quad (26)
\end{aligned}$$

3.2 Top quark width and hard photon radiation

We must also consider the amplitude with real photon emission off the t quark, see Fig. 12. This amplitude involves a propagator with denominator

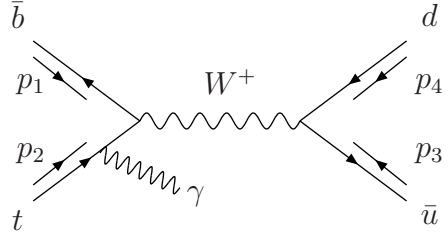


Fig. 12. The top Bremsstrahlung diagram

$(p_2 - p_5)^2 + m_t^2 - i m_t \Gamma_t$ which evaluates to $z_2 - i m_t \Gamma_t$ with $z_2 = -2p_2 \cdot p_5$.

The amplitude of the hard photon radiation process without taking account of the top quark width can be presented in the following form:

$$\mathcal{A}_\gamma^{(0)} = \mathcal{A}_t^{(0)} + \mathcal{A}_{udbW}. \quad (27)$$

Here $\mathcal{A}_t^{(0)}$ is the amplitude of the radiating top quark and \mathcal{A}_{udbW} is the rest. The amplitude (27) is gauge invariant: $\mathcal{A}_\gamma^{(0)} \cdot p_5 = 0$.

One can define the amplitude of the hard photon radiation process taking account of the top quark width as

$$\mathcal{A}_\gamma = \mathcal{A}_t + \mathcal{A}_{udbW} = \frac{z_2}{z_2 - i m_t \Gamma_t} \mathcal{A}_t^{(0)} + \mathcal{A}_{udbW}, \quad (28)$$

where the top quark propagator with width Γ_t was introduced.

The amplitude (28) destroys gauge invariance: $\mathcal{A}_\gamma \cdot p_5 \neq 0$. The gauge violation is of order Γ_t/m_t .

To recover gauge invariance one can modify the amplitude (28) in the following way:

$$\begin{aligned}\mathcal{A}_\gamma &\rightarrow \mathcal{A}'_\gamma = \frac{z_2}{z_2 - im_t \Gamma_t} \mathcal{A}_\gamma^{(0)} \\ &= \frac{z_2}{z_2 - im_t \Gamma_t} \left[\mathcal{A}_t^{(0)} + \mathcal{A}_{udbW} \right].\end{aligned}\quad (29)$$

Such transformation (called *overall scheme, (o)*) obviously leads to gauge invariance and the mod-squared amplitude will have the form

$$\begin{aligned}|\mathcal{A}_\gamma^{over}|^2 &= \frac{z_2^2}{z_2^2 + m_t^2 \Gamma_t^2} \left\{ \left| \mathcal{A}_t^{(0)} \right|^2 \right. \\ &\quad + \left[\left(\mathcal{A}_t^{(0)} \right)^* \mathcal{A}_{udbW} + \mathcal{A}_t^{(0)} (\mathcal{A}_{udbW})^* \right] \\ &\quad \left. + |\mathcal{A}_{udbW}|^2 \right\}.\end{aligned}\quad (30)$$

As is seen from equation (30), all terms are now regularized by the top quark width but the last term is multiplied by an *artificial* factor which cannot be treated in the soft (Born-like) kinematics.

To avoid the problem with integration one can introduce a new *gauge non-invariant* amplitude (which we call *fixed₁ scheme (f₁)*):

The amplitude \mathcal{A}_γ with top quark width introduced *ab initio* (28) is called *fixed₁*:

$$\begin{aligned}|\mathcal{A}_\gamma^{fixed_1}|^2 &= \frac{z_2^2}{z_2^2 + m_t^2 \Gamma_t^2} \left| \mathcal{A}_t^{(0)} \right|^2 \\ &\quad + 2\text{Re} \frac{z_2}{z_2 - im_t \Gamma_t} \mathcal{A}_t^{(0)} (\mathcal{A}_{udbW})^* \\ &\quad + |\mathcal{A}_{udbW}|^2.\end{aligned}\quad (31)$$

An alternative version, called *fixed₂*, obtains by setting equal to one the coefficient of $|\mathcal{A}_{udbW}|^2$ in Eq. (30):

$$|\mathcal{A}_\gamma^{fixed_2}|^2 = \frac{z_2^2}{z_2^2 + m_t^2 \Gamma_t^2} \left\{ \left| \mathcal{A}_t^{(0)} \right|^2 \right.$$

$$\begin{aligned}&\quad + \left[\left(\mathcal{A}_t^{(0)} \right)^* \mathcal{A}_{udbW} + \mathcal{A}_t^{(0)} (\mathcal{A}_{udbW})^* \right] \Big\} \\ &\quad + |\mathcal{A}_{udbW}|^2.\end{aligned}\quad (32)$$

In the next chapter we present numerical results for all width schemes introduced above in order to estimate the numerical impact of gauge violation in *fixed schemes*.

4 Numerical Results

In this section we present the **SANC** results for the cross sections of single top quark production and for the decay widths of the top quark. The tree level contributions, both Born and single real photon emission, are compared with **CompHEP** [19]. All numerical results for this section were produced with the standard **SANC INPUT** working in the $\alpha(0)$ EW scheme, if not stated otherwise.

The standard **SANC** input parameters set reads:

$$\begin{aligned}G_F &= 1.16637 \times 10^{-5} \text{ GeV}^{-2}, \\ \alpha(0) &= 1/137.035999, & \alpha_s &= 0.00729735257, \\ M_W &= 80.403 \text{ GeV}, & \Gamma_W &= 2.141 \text{ GeV}, \\ M_Z &= 91.1876 \text{ GeV}, & \Gamma_Z &= 2.4952 \text{ GeV}, \\ M_H &= 120 \text{ GeV}, & m_t &= 174.2 \text{ GeV}, \\ m_u &= 62 \text{ MeV}, & m_d &= 83 \text{ MeV}, \\ m_c &= 1.5 \text{ GeV}, & m_s &= 215 \text{ MeV}, \\ m_t &= 174.2 \text{ GeV}, & m_b &= 4.7 \text{ GeV}, \\ |V_{ud}| &= 1, & |V_{cs}| &= 1, \\ |V_{us}| &= 0, & |V_{cd}| &= 0, \\ |V_{tb}| &= 1.\end{aligned}\quad (33)$$

This section is subdivided into three subsections: for the decay channel, s channel and t channel; for the latter subprocesses results for both *direct* ($bu \rightarrow td$) and *crossed* ($b\bar{d} \rightarrow t\bar{u}$) channels are presented separately.

Each subsection, in turn, consists of two paragraphs. The first paragraphs contain a comparison with CompHEP of the Born cross section and of the hard photon contribution with a cut on photon energy E_γ in the rest frame of the top (for decay channel) and in the cms of the initial particles for s and t channels.

In the second paragraphs we present a study of complete EWRC at the partonic level. We show the decay widths for the decay channel and cross sections for the reactions at the tree and one-loop levels. The one-loop EWRC is defined as usual:

$$\delta = \frac{\mathcal{O}^{\text{1loop}} - \mathcal{O}^{\text{tree}}}{\mathcal{O}^{\text{tree}}}, \quad (34)$$

where \mathcal{O} is either width (Γ) or cross section (σ).

Furthermore, the dimensionless soft-hard separator $\bar{\omega}$ subdivides soft and hard real photon contributions. Their sum does not depend on $\bar{\omega}$.

For decays $a \rightarrow b + c + d + \gamma$ with $s = -(p_a - p_b)^2$ and $s' = M_{c,d}^2$ and for the processes, $a + b \rightarrow c + d + \gamma$ with $s = M_{a,b}^2$ and $s' = M_{c,d}^2$

$$\bar{\omega} = 1 - \frac{s'}{s}, \quad \text{and} \quad E_\gamma \geq \frac{s}{2} \bar{\omega}. \quad (35)$$

For each of the four channels we present Tables illustrating the existence of an E_γ ($\bar{\omega}$) stability plateau for two options $\Gamma_t = 0, \neq 0$, and answering the question how big the difference is of the EWRC between

the two Γ_t options. For reactions, we also investigate the question of the initial quark masses (m_q) independence of the subtracted quantities.

For the explanation of the necessity of the subtraction procedure and its realization in the \overline{MS} scheme within SANC we refer to our earlier papers [20]–[21].

4.1 Decay Channel $t \rightarrow b + u + \bar{d}$

4.1.1 SANC–CompHEP comparison

No new comparison for this channel was done compared to Ref. [2]. If the top quark width is taken into account, SANC and CompHEP numbers agree well.

4.1.2 One-loop EW corrections

Process $t \rightarrow b + \mu^+ + \bar{\nu}_\mu$.

$\Gamma^{\text{Born}}=0.1490949(2) \text{ GeV}$			
$\Gamma_t = 0$			
$E_\gamma, \text{ GeV}$	10^{-1}	10^{-2}	10^{-3}
Γ^{1loop}	0.159503(1)	0.159495(2)	0.159499(7)
δ	6.981(1)	6.975(1)	6.978(5)
$\Gamma_t \neq 0, \text{ fixed}_1$			
Γ^{1loop}	0.160736(2)	0.160784(2)	0.160787(8)
δ	7.810(1)	7.841(2)	7.842(5)

Table 1. The total lowest-order and one-loop corrected widths Γ^{Born} and Γ^{1l} in GeV and relative one-loop correction δ in % for $E_\gamma = 10^{-1}, 10^{-2}, 10^{-3} \text{ GeV}$.

As is seen from Table 1, there is good $\bar{\omega}$ stability for $E_\gamma \leq 10^{-2}$ GeV and about +0.9% increase of the EWRC for this partial decay width if one uses $\Gamma_t \neq 0$ option as compared to the $\Gamma_t = 0$ one.

Process $t \rightarrow b + u + \bar{d}$.

$\Gamma^{\text{Born}}=0.4472847(7)$ GeV			
$\Gamma_t = 0$			
E_γ , GeV	10^{-1}	10^{-2}	10^{-3}
Γ^{1loop}	0.47922(1)	0.47920(1)	0.47918(1)
δ	7.139(1)	7.135(1)	7.131(3)
$\Gamma_t \neq 0$, <i>fixed</i> ₁			
Γ^{1loop}	0.48293(1)	0.48312(1)	0.48311(1)
δ	7.969(1)	8.012(1)	8.010(2)

Table 2. The same but for $t \rightarrow b + u + \bar{d}$ process.

As is seen from Table 2, one can draw similar conclusions for both considered partial decay channels.

4.2 s channel

There are two generic s channel processes:

$$\bar{d} + u \rightarrow \bar{b} + t, \quad \text{and} \quad \bar{u} + d \rightarrow \bar{t} + b. \quad (36)$$

4.2.1 SANC–CompHEP comparison

It is sufficient to consider only one: $\bar{u} + d \rightarrow \bar{t} + b$. For this comparison we use the **CompHEP** (v.4.5.1) setup with a cut on the cms photon energy $E_\gamma \geq 2$ GeV.

\sqrt{s}/GeV	ws	200	1000	7000
$\Gamma_t = 0$				
CompHEP		8.172(1)	17.19(1)	0.7966(2)
SANC		8.173(1)	17.19(1)	0.7964(1)
$\Gamma_t = 1.54688$ GeV				
CompHEP	o	7.835(1)	16.93(1)	0.7882(1)
	f	7.788(1)	16.90(1)	0.7884(1)
SANC	o	7.834(1)	16.93(1)	0.7885(1)
	f ₁	7.788(1)	16.91(1)	0.7884(1)
	f ₂	7.787(1)	16.91(1)	0.7884(1)

Table 3. Comparison of the cross section $\sigma^{\text{hard}}(\sqrt{s}, \bar{\omega})$ (fb) for three cms energies, two options: $\Gamma_t = 0, \neq 0$, and three *width schemes* (ws): *o*-overall, *f*-fixed (f₁₍₂₎=*fixed*₁₍₂₎) for the case of **SANC**.

As is seen from Table 3, there is good agreement of numbers obtained from **SANC** and **CompHEP** within the statistical errors for all considered options and cms energies. It is worth to note that the two versions of width schemes agree well for all energies except near the threshold and that the *fixed*₁ scheme agrees with the **CompHEP** *fixed* scheme as expected.

4.2.2 One-loop EW corrections

The numbers of this subsection are produced with **SANC** setup, Eq. (33). The aim is to demonstrate the intervals of stability of one-loop corrected EW cross sections σ^{1loop} and relative EWRC δ against variation

of the soft-hard separation parameter, $\bar{\omega}$ and to study the difference between the two options: $\Gamma_t = 0, \neq 0$.

$\sqrt{s}=200$ GeV, $\sigma^{\text{Born}}=0.30809055(1)$ pb			
$\Gamma_t = 0$			
$\bar{\omega}$	10^{-4}	10^{-5}	10^{-6}
$\hat{\sigma}^{\text{1loop}}$	0.315169(2)	0.315167(3)	0.315167(4)
δ	2.297(1)	2.297(1)	2.297(1)
$\Gamma_t \neq 0, \text{fixed}_1$			
$\hat{\sigma}^{\text{1loop}}$	0.315469(2)	0.315471(3)	0.315472(3)
δ	2.395(1)	2.396(1)	2.396(1)

Table 4. The total lowest-order cross sections $\hat{\sigma}^{\text{Born}}$, the one-loop corrected cross sections $\hat{\sigma}^{\text{1loop}}$ in pb and relative corrections δ in % at three values of $\bar{\omega} = 10^{-4}, 10^{-5}, 10^{-6}$ and two of Γ_t .

$\sqrt{s}=1000$ GeV, $\sigma^{\text{Born}}=0.105977185(2)$ pb			
$\Gamma_t = 0$			
$\bar{\omega}$	10^{-4}	10^{-5}	10^{-6}
$\hat{\sigma}^{\text{1loop}}$	0.102872(3)	0.102874(3)	0.102875(4)
δ	-2.930(2)	-2.928(3)	-2.927(4)
$\Gamma_t \neq 0, \text{fixed}_1$			
$\hat{\sigma}^{\text{1loop}}$	0.102753(3)	0.102775(4)	0.102774(5)
δ	-3.043(3)	-3.021(3)	-3.023(4)

Table 5. The same but for $\sqrt{s}=1000$ GeV.

Tables 4–6 were computed with three values of $\bar{\omega}$ and for two options $\Gamma_t = 0, \neq 0$. As far as $\bar{\omega}$ -stability is concerned, we see that it depends on the Γ_t -option.

$\sqrt{s}=7000$ GeV, $\sigma^{\text{Born}}=2.23529503(4)$ fb			
$\Gamma_t = 0$			
$\bar{\omega}$	10^{-5}	10^{-6}	10^{-7}
$\hat{\sigma}^{\text{1loop}}$	1.5917(1)	1.5917(2)	1.5919(1)
δ	-28.79(1)	-28.80(1)	-28.78(1)
$\Gamma_t \neq 0, \text{fixed}_1$			
$\hat{\sigma}^{\text{1loop}}$	1.5815(1)	1.5895(2)	1.5895(2)
δ	-29.25(1)	-28.89(1)	-28.89(1)

Table 6. The same but for $\sqrt{s}=7000$ GeV and for $\bar{\omega} = 10^{-5}, 10^{-6}, 10^{-7}$ and the cross sections given in fb.

For $\Gamma_t = 0$ there is stability for all considered \sqrt{s} and $\bar{\omega}$. For $\Gamma_t \neq 0$ it depends on the cms energy \sqrt{s} : for 200 GeV stability sets in already at $\bar{\omega} = 10^{-4}$, for 1000 GeV at $\bar{\omega} = 10^{-5}$ and for 7000 GeV at $\bar{\omega} = 10^{-6}$.

$\sqrt{s}=200$ GeV, $\Gamma_t = 0$			
$\bar{\omega}$	10^{-4}	10^{-5}	10^{-6}
$\hat{\sigma}_1^{\overline{MS}}$	0.328077(2)	0.328082(4)	0.328083(4)
$\delta_1^{\overline{MS}}$	6.487(1)	6.489(1)	6.489(1)
$\hat{\sigma}_2^{\overline{MS}}$	0.328073(2)	0.328078(2)	0.328076(3)
$\delta_2^{\overline{MS}}$	6.486(1)	6.488(1)	6.487(1)

Table 7. The total one-loop corrected \overline{MS} subtracted quantities $\hat{\sigma}^{\overline{MS}}$ in pb and corresponding $\delta^{\overline{MS}}$ in % at $\bar{\omega} = 10^{-4}, 10^{-5}, 10^{-6}$, respectively. Subscript 1 means that light quark masses are used as in Eq. (33), while 2 means that 10 times smaller masses are used.

However, one can see that the difference between the two options, although it persists, is of order 1 per mille in absolute deviation, which is well below any reasonable estimate of the theoretical uncertainty. We therefore conclude that one may use the usual infrared regularization for s channel processes.

The numbers of Tables 7–9 were produced with the aim to demonstrate the independence from light quark masses of the subtracted quantities, $\hat{\sigma}^{\overline{MS}}$ and $\delta^{\overline{MS}}$ for $\Gamma_t = 0$ option at three cms energies. One sees that the light quark mass independence holds in all considered cases at the level much lower than 1 per mille, which is quite sufficient for practical applications.

$\sqrt{s}=1000$ GeV, $\Gamma_t = 0$			
$\bar{\omega}$	10^{-4}	10^{-5}	10^{-6}
$\hat{\sigma}_1^{\overline{MS}}$	0.100084(3)	0.100086(3)	0.100087(4)
$\delta_1^{\overline{MS}}$	-5.561(2)	-5.559(3)	-5.558(4)
$\hat{\sigma}_2^{\overline{MS}}$	0.100084(3)	0.100086(3)	0.100087(4)
$\delta_2^{\overline{MS}}$	-5.565(4)	-5.567(5)	-5.568(7)

Table 8. The same but for $\sqrt{s}=1000$ GeV.

4.3 t channel

4.3.1 SANC–CompHEP comparison

This is the most complicated case: t channel cross sections usually show up bad statistical convergence. For this comparison we use the **CompHEP** (v.4.5.1)

$\sqrt{s}=7000$ GeV, $\Gamma_t = 0$			
$\bar{\omega}$	10^{-5}	10^{-6}	10^{-7}
$\hat{\sigma}_1^{\overline{MS}}$	1.4566(1)	1.4565(2)	1.4568(1)
$\delta_1^{\overline{MS}}$	-34.84(1)	-34.84(1)	-34.83(1)
$\hat{\sigma}_2^{\overline{MS}}$	1.4569(2)	1.4570(2)	1.4570(2)
$\delta_2^{\overline{MS}}$	-34.82(1)	-34.82(1)	-34.82(1)

Table 9. The same but for $\sqrt{s}=7000$ GeV but for cross sections given in fb and for $\bar{\omega} = 10^{-5}, 10^{-6}, 10^{-7}$.

setup, but with non-zero masses of the u and d quarks (accessed via $bc \rightarrow ts\gamma$ channel). For the Tables of this subsection we used $m_u = m_d = m_q = 66$ MeV, and $10m_q$ means $m_u = m_d = 660$ MeV. The cut on the cms photon energy was $E_\gamma \geq 2$ GeV.

Furthermore, rows marked “SANC(S)” were computed retaining m_q or $10m_q$ only in fermion propagators radiating a photon, while “SANC(F)” means that light quark masses were kept everywhere (“F”ully massive case). Table 11 contains the same information as Table 10 but for the process $b + \bar{d} \rightarrow t + \bar{u}$.

Let us discuss the results of Tables 10–11 which are qualitatively the same, so we need not refer to the Table number.

Two options ($\Gamma_t = 0, \neq 0$) \otimes (m_q) (4 upper rows) show very good agreement at the threshold, $\sqrt{s} = 200$ GeV, and a notable deviation at TeV energies. We assumed that this is due to the mass singular origin of external light quark lines emitting photons, which obviously is getting worse at high energies. In this con-

$\sqrt{\hat{s}}/GeV$	ws	200	1000	7000
$\Gamma_t = 0, m_q$				
CompHEP		0.2468(1)	9.078(1)	18.68(1)
SANC(S)		0.2467(1)	9.090(1)	18.45(1)
$\Gamma_t \neq 0, m_q$				
CompHEP	f	0.2392(1)	9.161(1)	18.68(1)
SANC(S)	f ₁	0.2392(1)	9.174(1)	18.70(1)
$\Gamma_t = 0, 10m_q$				
CompHEP		0.1740(1)	7.512(1)	16.11(1)
SANC(S)		0.1745(1)	7.514(1)	16.12(1)
SANC(F)		0.1740(1)	—	—
$\Gamma_t \neq 0, 10m_q$				
CompHEP	f	0.1694(1)	7.597(1)	16.36(1)
SANC(S)	f ₁	0.1698(1)	7.599(1)	16.37(1)
SANC(F)	f ₁	0.1694(1)	—	—

Table 10. Comparison of the cross section $\sigma^{\text{hard}}(\sqrt{\hat{s}}, \bar{\omega})$, fb for the process $b + u \rightarrow t + d$ for three cms energies; four options: $(\Gamma_t = 0, \neq 0) \otimes (m_q, 10m_q)$; and *fixed width scheme* (*ws*): ($f_1 = \text{fixed}_1$ for the case of **SANC**).

nection, we emphasize that a special procedure of numerical stabilization of terms giving rise to light quark mass singularities was applied in **SANC**.

To check this assumption we considered options $(\Gamma_t = 0, \neq 0) \otimes (10m_q)$ and we immediately see the inverse trend: only satisfactory agreement at $\sqrt{\hat{s}} = 200$ GeV and much better agreement at TeV energies.

This exercise convinced us that in the mass singular stable regime (large masses) **CompHEP** and **SANC** results

$\sqrt{\hat{s}}/GeV$	ws	200	1000	7000
$\Gamma_t = 0, m_q$				
CompHEP		0.1562(1)	8.620(1)	18.27(1)
SANC		0.1562(2)	8.634(1)	18.33(1)
$\Gamma_t \neq 0, m_q$				
CompHEP	f	0.1522(1)	8.706(1)	18.53(1)
SANC	f ₁	0.1522(1)	8.717(1)	18.57(1)
$\Gamma_t = 0, 10m_q$				
CompHEP		0.1032(1)	7.120(1)	15.98(1)
SANC		0.1037(1)	7.123(1)	15.98(1)
SANC(F)		0.1032(1)	—	—
$\Gamma_t \neq 0, 10m_q$				
CompHEP	f	0.1009(1)	7.204(1)	16.22(1)
SANC	f ₁	0.1014(1)	7.207(1)	16.24(1)
SANC(F)	f ₁	0.1009(1)	—	—

Table 11. The same comparison of the cross section $\sigma^{\text{hard}}(\sqrt{\hat{s}}, \bar{\omega})$, fb but for the process $b + \bar{d} \rightarrow t + \bar{u}$.

do agree. It is easy to understand why with the latter options the situation near the threshold is not so ideal. In **SANC** we want to neglect terms with power dependence on light quark masses, keeping only those that would lead to mass singularities. Relatively large masses, $10m_q$, start to matter near the threshold. (Note also that on passing to the hadronic level we will need to subtract mass quark singularities anyway: see next subsection).

To check this assumption we considered the fully massive variant **SANC(F)** with options $(\Gamma_t = 0, \neq 0) \otimes$

($10m_q$) and only at $\sqrt{\hat{s}} = 200$ GeV. As is seen from the **SANC(F)** rows of the Tables, the good agreement with **CompHEP** is recovered.

Although **SANC(F)** is identical to **CompHEP**, we prefer to use the much faster **SANC(S)** version of the code since the masses of u , d and s quarks are very small. The only exception is the c quark whose mass effect will be obviously notable near the threshold. Since we possess the **SANC(F)** version of the code, we can use a mixed variant with only c quark mass dependence retained.

To conclude this section, we note that the results for the charge conjugate channels are identical to those we have considered:

$$\begin{aligned} \bar{b} + \bar{u} &\rightarrow \bar{t} + \bar{d} \quad \text{to} \quad b + u \rightarrow t + d, \\ \bar{b} + d &\rightarrow \bar{t} + u \quad \text{to} \quad b + \bar{d} \rightarrow t + \bar{u}. \end{aligned} \quad (37)$$

4.3.2 One-loop EW corrections, process $bu \rightarrow td$

The numerical results for this subsection were again produced with the **SANC** setup, Eq. (33), with the same aim to demonstrate the stability of one-loop corrected EW cross sections σ^{1loop} and relative EWRC δ against variation of the soft-hard separator $\bar{\omega}$ and to study the difference between the two options: $\Gamma_t = 0, \neq 0$.

Tables 12–14 were computed with three values of $\bar{\omega}$ and for two options $\Gamma_t = 0, \neq 0$. As is seen, the intervals of $\bar{\omega}$ -stability depend on $\sqrt{\hat{s}}$. The higher the

$\sqrt{\hat{s}}=200$ GeV, $\sigma^{\text{Born}}=7.3551155(1)$ pb			
$\Gamma_t = 0$			
$\bar{\omega}$	10^{-4}	10^{-5}	10^{-6}
$\hat{\sigma}^{\text{1loop}}$	7.81964(2)	7.81954(4)	7.81956(4)
δ	6.3156(3)	6.3144(5)	6.3146(6)
$\Gamma_t \neq 0, \text{fixed}_1$			
$\hat{\sigma}^{\text{1loop}}$	7.81954(2)	7.81956(3)	7.81957(4)
δ	6.3143(3)	6.3145(4)	6.3147(5)

Table 12. The total lowest-order cross sections $\hat{\sigma}^{\text{Born}}$, the one-loop corrected cross sections $\hat{\sigma}^{\text{1loop}}$ in pb and relative one-loop correction δ in % at three values of $\bar{\omega} = 10^{-4}, 10^{-5}, 10^{-6}$ and two values of Γ_t .

$\sqrt{\hat{s}}=1000$ GeV, $\sigma^{\text{Born}}=48.99340951(6)$ pb			
$\Gamma_t = 0$			
$\bar{\omega}$	10^{-5}	10^{-6}	10^{-7}
$\hat{\sigma}^{\text{1loop}}$	53.344(1).	53.345(1).	53.346(1).
δ	8.880(1).	8.881(2).	8.883(2).
$\Gamma_t \neq 0, \text{fixed}_1$			
$\hat{\sigma}^{\text{1loop}}$	53.292(1)	53.293(1)	53.293(1)
δ	8.773(1)	8.776(2)	8.776(2)

Table 13. The same but for $\sqrt{\hat{s}}=1000$ GeV and for $\bar{\omega} = 10^{-5}, 10^{-6}, 10^{-7}$.

cms energy, the lower are the values of $\bar{\omega}$ required to reach stability. For $\sqrt{\hat{s}}=200$ GeV, stability starts at $\bar{\omega} = 10^{-4}$, for $\sqrt{\hat{s}}=1000$ GeV at $\bar{\omega} = 10^{-5}$ and for $\sqrt{\hat{s}}=7000$ TeV it depends additionally on the Γ_t -option. For $\Gamma_t = 0$ stability starts at $\bar{\omega} = 10^{-6}$ but

$\sqrt{s}=7000$ GeV, $\sigma^{\text{Born}}=50.82423111(8)$ pb			
$\Gamma_t = 0$			
$\bar{\omega}$	10^{-6}	10^{-7}	10^{-8}
$\hat{\sigma}^{\text{1loop}}$	55.696(2)	55.697(2)	55.697(2)
δ	9.586(3)	9.588(4)	9.587(4)
$\Gamma_t \neq 0$, <i>fixed</i> ₁			
$\hat{\sigma}^{\text{1loop}}$	55.613(1)	55.639(2)	55.640(2)
δ	9.428(3)	9.474(3)	9.476(4)

Table 14. The same but for $\sqrt{s}=7000$ GeV and for $\bar{\omega} = 10^{-6}, 10^{-7}, 10^{-8}$.

for $\Gamma_t \neq 0$ only at $\bar{\omega} = 10^{-7}$. However, one can see that the difference between the two options, although it persists, is well below 1 per mille in absolute deviation at lower energies, reaching 1 per mille only at $\sqrt{s}=7000$ GeV, that is the difference under study is below any reasonable estimate of the theoretical uncertainty. We therefore conclude that one may use the usual infrared regularization also for t channel processes.

Subtraction of quark mass singularities

The numbers of the Tables 15–17 were produced with the aim to demonstrate the light quark mass independence of the one-loop subtracted quantities $\hat{\sigma}^{\overline{MS}}$ and $\delta^{\overline{MS}}$ for the $\Gamma_t = 0$ option at three cms energies and three values of $\bar{\omega}$.

The stability of $\hat{\sigma}^{\overline{MS}}$ and $\delta^{\overline{MS}}$ seen in Tables 15–17 is a very important check of the correctness of imple-

$\sqrt{s}=200$ GeV, $\sigma^{\text{Born}}=7.3551155(1)$ pb			
$\Gamma_t = 0$			
$\bar{\omega}$	10^{-4}	10^{-5}	10^{-6}
$\hat{\sigma}_1^{\overline{MS}}$	8.09370(2)	8.09377(4)	8.09380(4)
$\delta_1^{\overline{MS}}$	10.042(1)	10.043(1)	10.043(1)
$\hat{\sigma}_2^{\overline{MS}}$	8.09116(4)	8.09127(6)	8.09129(8)
$\delta_2^{\overline{MS}}$	10.043(1)	10.045(1)	10.045(1)

Table 15. The total one-loop corrected \overline{MS} subtracted quantities (see text) $\hat{\sigma}^{\overline{MS}}$ in pb and corresponding $\delta^{\overline{MS}}$ in % at $\bar{\omega} = 10^{-4}, 10^{-5}, 10^{-6}$. Sub-index 1 means that light quark masses used are as in Eq. (33), while 2 means that 10 times lower masses are used.

$\sqrt{s}=1000$ GeV, $\sigma^{\text{Born}}=48.99340953(6)$ pb			
$\Gamma_t = 0$			
$\bar{\omega}$	10^{-5}	10^{-6}	10^{-7}
$\hat{\sigma}_1^{\overline{MS}}$	53.416(1)	53.416(1)	53.417(1)
$\delta_1^{\overline{MS}}$	9.027(1)	9.028(2)	9.030(2)
$\hat{\sigma}_2^{\overline{MS}}$	53.416(1)	53.416(1)	53.417(2)
$\delta_2^{\overline{MS}}$	9.029(2)	9.029(2)	9.032(3)

Table 16. The same but for $\sqrt{s}=1000$ GeV and for $\bar{\omega} = 10^{-5}, 10^{-6}, 10^{-7}$.

mentation of the complete EWRC and of the initial quark mass singularity subtraction. The latter is crucial at the envisaged stage of going to the hadron level, i.e. convolution with parton density functions.

$\sqrt{s}=7000 \text{ GeV}, \sigma^{\text{Born}}=50.82423111(8) \text{ pb}$			
$\Gamma_t = 0$			
$\bar{\omega}$	10^{-6}	10^{-7}	10^{-8}
$\hat{\sigma}_1^{\overline{MS}}$	55.699(2)	55.700(2)	55.699(2)
$\delta_1^{\overline{MS}}$	9.591(3)	9.593(4)	9.592(4)
$\hat{\sigma}_2^{\overline{MS}}$	55.698(2)	55.697(3)	55.696(3)
$\delta_2^{\overline{MS}}$	9.589(3)	9.588(5)	9.585(6)

Table 17. The same but for $\sqrt{s}=7000 \text{ GeV}$ and for $\bar{\omega} = 10^{-6}, 10^{-7}, 10^{-8}$.

4.3.3 One-loop EW corrections: process $b\bar{d} \rightarrow t\bar{u}$

Here we repeat the study of subsection 4.3.2, but now for the crossed t channel. Tables 18–20 are analogous to Tables 12–14. They demonstrate the stability of $\hat{\sigma}^{11}$ and σ^{11} against variation of $\bar{\omega}$ and show the difference between the options $\Gamma_t = 0, \neq 0$.

Tables 18–20 show up properties very similar to the Tables for the direct t channel. Each Table shows the presence of a plateau of stability in $\bar{\omega}$ and the same level of difference between calculations for two options $\Gamma_t = 0, \neq 0$, qualitatively with very similar energy dependence.

Subtraction of quark mass singularities

The numbers of Tables 21–23 were also produced with the aim to demonstrate the light quark mass independence of the subtracted quantities $\hat{\sigma}^{\overline{MS}}$ and $\delta^{\overline{MS}}$ for option $\Gamma_t = 0$ at three cms energies.

$\sqrt{s}=200 \text{ GeV}, \sigma^{\text{Born}}=4.495790646(3) \text{ pb}$			
$\Gamma_t = 0$			
$\bar{\omega}$	10^{-4}	10^{-5}	10^{-6}
$\hat{\sigma}^{1\text{loop}}$	4.87169(2)	4.87165(2)	4.87165(3)
δ	8.3612(4)	8.3603(5)	8.3603(7)
$\Gamma_t \neq 0, \text{fixed}_1$			
$\hat{\sigma}^{1\text{loop}}$	4.86989(5)	4.86990(2)	4.86991(3)
δ	8.3212(4)	8.3213(5)	8.3215(6)

Table 18. The total lowest-order cross sections $\hat{\sigma}^{\text{Born}}$, the one-loop corrected cross sections $\hat{\sigma}^{1\text{loop}}$ in pb and relative one-loop correction δ in % at three values of $\bar{\omega} = 10^{-4}, 10^{-5}, 10^{-6}$ and two values of Γ_t .

$\sqrt{s}=1000 \text{ GeV}, \sigma^{\text{Born}}=46.68695597(6) \text{ pb}$			
$\Gamma_t = 0$			
$\bar{\omega}$	10^{-5}	10^{-6}	10^{-7}
$\hat{\sigma}^{1\text{loop}}$	51.054(1)	51.054(1)	51.055(1)
δ	9.354(1)	9.354(2)	9.356(2)
$\Gamma_t \neq 0, \text{fixed}_1$			
$\hat{\sigma}^{1\text{loop}}$	51.004(1)	51.005(1)	51.006(1)
δ	9.246(1)	9.249(2)	9.250(2)

Table 19. The same but for $\sqrt{s}=1000 \text{ GeV}$ and for $\bar{\omega} = 10^{-5}, 10^{-6}, 10^{-7}$.

Again, Tables 21–23, although within larger statistical errors, show the stability of $\hat{\sigma}^{\overline{MS}}$ and $\delta^{\overline{MS}}$ for all cms energies and $\bar{\omega}$ values considered, confirming the correctness of implementation of the complete EWRC also for the case of the crossed t channel.

$\sqrt{s}=7000$ GeV, $\sigma^{\text{Born}}=50.72449055(7)$ pb			
$\Gamma_t = 0$			
$\bar{\omega}$	10^{-6}	10^{-7}	10^{-8}
$\hat{\sigma}^{\text{1loop}}$	55.581(2)	55.583(2)	55.580(2)
δ	9.575(3)	9.578(4)	9.572(4)
$\Gamma_t \neq 0, \text{fixed}_1$			
$\hat{\sigma}^{\text{1loop}}$	55.495(2)	55.527(2)	55.528(2)
δ	9.404(3)	9.467(3)	9.469(4)

Table 20. The same but for $\sqrt{s}=7000$ GeV and for $\bar{\omega} = 10^{-6}, 10^{-7}, 10^{-8}$.

$\sqrt{s}=200$ GeV, $\sigma^{\text{Born}}=4.495790646(3)$ pb			
$\Gamma_t = 0$			
$\bar{\omega}$	10^{-4}	10^{-5}	10^{-6}
$\hat{\sigma}_1^{\overline{MS}}$	4.92749(2)	4.92749(2)	4.92749(3)
$\delta_1^{\overline{MS}}$	9.6023(4)	9.6023(5)	9.6023(7)
$\hat{\sigma}_2^{\overline{MS}}$	4.92515(3)	4.92513(4)	4.92514(5)
$\delta_2^{\overline{MS}}$	9.6065(6)	9.6061(9)	9.606(1)

Table 21. The total one-loop corrected \overline{MS} subtracted quantities $\hat{\sigma}^{\overline{MS}}$ in pb and corresponding $\delta^{\overline{MS}}$ in % at $\bar{\omega} = 10^{-4}, 10^{-5}, 10^{-6}$. Sub-index 1 means that light quark masses used are as in Eq. (33), while 2 means that 10 times lower masses are used.

5 Conclusions and Outlook

In this paper we describe the implementation into the SANC framework of the complete one-loop EW calculations, including hard bremsstrahlung contributions, for the processes of the top quark decays a of s and

$\sqrt{s}=1000$ GeV, $\sigma^{\text{Born}}=46.68695597(6)$ pb			
$\Gamma_t = 0$			
$\bar{\omega}$	10^{-5}	10^{-6}	10^{-7}
$\hat{\sigma}_1^{\overline{MS}}$	51.086(6)	51.0858(8)	51.087(1)
$\delta_1^{\overline{MS}}$	9.422(1)	9.422(2)	9.424(2)
$\hat{\sigma}_2^{\overline{MS}}$	51.0856(9)	51.086(1)	51.087(2)
$\delta_2^{\overline{MS}}$	9.424(2)	9.424(3)	9.428(3)

Table 22. The same but for $\sqrt{s}=1000$ GeV and for $\bar{\omega} = 10^{-5}, 10^{-6}, 10^{-7}$.

$\sqrt{s}=7000$ GeV, $\sigma^{\text{Born}}=50.72449055(7)$ pb			
$\Gamma_t = 0$			
$\bar{\omega}$	10^{-6}	10^{-7}	10^{-8}
$\hat{\sigma}_1^{\overline{MS}}$	55.583(2)	55.585(2)	55.582(2)
$\delta_1^{\overline{MS}}$	9.579(3)	9.582(4)	9.575(4)
$\hat{\sigma}_2^{\overline{MS}}$	55.583(2)	55.585(3)	55.576(3)
$\delta_2^{\overline{MS}}$	9.579(4)	9.582(5)	9.564(7)

Table 23. The same but for $\sqrt{s}=7000$ GeV and for $\bar{\omega} = 10^{-6}, 10^{-7}, 10^{-8}$.

t channel production, the latter two at the partonic level,. The essentially new aspect of this paper is the study of regularisation of the top quark–photon infrared divergences with aid of the complex mass of the top quark. For this reason, we briefly come back to the top decay channels, since this issue was not studied in our previous papers, Ref. [1,2]. A comparison of these electroweak corrections computed within this new approach with those computed by the con-

ventional method showed a sizable (1%) effect for top decays and only per mille level effect for both considered top production processes. In this paper we limit ourselves to 4-fermion type of processes. For this reason we do not consider t quark production channel in association with W boson. This channel will be presented elsewhere.

We have presented analytical expressions for the covariant amplitude of the process and the helicity amplitudes for three different cross channels within the standard **SANC** multichannel approach, Ref [17]. In this approach the one-loop covariant amplitude is computed only once for to-the-vacuum-annihilation processes, see Figs. 1 and 2. To get the CA for a physical channel a cross transformation of external 4-momenta is performed. The helicity amplitudes have been calculated for each channel separately.

Within the **SANC** framework, we have created the standard FORM and FORTRAN modules, see, Ref. [22], compiled into a package `sanc_cc_v1.40` which may be downloaded from **SANC** project homepages. All the calculations were done using a combination of analytic and Monte Carlo integration methods which will make it easy to impose experimental cuts in forthcoming calculations for the pp -collisions at LHC, which will be the subject of a subsequent paper.

The emphasis of this paper is to be assured of the correctness of our results. We observe the independence of the form factors on gauge parameters (all

calculations were done in R_ξ gauge), checked the stability of the result against variation of the soft-hard separation parameter $\bar{\omega}$ and the independence of the \overline{MS} subtracted quantities off the initial quark masses which is crucial for calculations at the hadronic level.

As has become **SANC** standard, we tried to compare our numerical results for these channels with other independent calculations. For the decay channels it was done in our previous papers (both EW [1] and QCD [23]), showing good agreement. As usual, the Born level and the hard photon contributions of all three channels were checked against **CompHEP** package and we found very good agreement for both $\Gamma_t = 0, \neq 0$ options.

As far as the comparison of EWRC for the production processes is concerned, the situation is not satisfactory. We did not find in the literature any calculations for the s channel. For the t channel there are many papers, see, for instance, Refs. [12–15] and references therein. The most appropriate is Ref. [12], where however the hard photon contribution is not included. We tried to suppress it in our calculations, but got only rough agreement with their Fig. 3(a). The most advanced paper Ref. [14] contains results at the hadronic level and, at present, we can not yet make a comparison.

The results presented in this papers lay a solid base for subsequent extensions of calculations for the single

top production channels at hadron colliders, basically LHC.

Acknowledgements. This work is partly supported by Russian Foundation for Basic Research grant N° 10-02-01030.

The authors are grateful to Gizo Nanava for a useful discussion on the subject of helicity amplitudes.

WvS is indebted to the directorate of the Dzhelapov Laboratory of Nuclear Problems, JINR, Dubna, for the hospitality extended to him during June 2010.

References

1. A. Arbuzov *et al.*, *Eur. Phys. J.* **C51** (2007) 585–591, [hep-ph/0703043](#).
2. D. Bardin *et al.*, *Phys. Part. Nucl. Lett.* **7** (2010) 72–79, [0903.1533](#).
3. A. Andonov *et al.*, *Comput. Phys. Commun.* **174** (2006) 481–517, [hep-ph/0411186](#).
4. D0 Collaboration, R. Schwienhorst, [0805.2175](#).
5. W. Bernreuther, *J. Phys.* **G35** (2008) 083001, [0805.1333](#).
6. D0 Collaboration, V. M. Abazov *et al.*, *Phys. Rev. Lett.* **98** (2007) 181802, [hep-ex/0612052](#).
7. D0 Collaboration, V. M. Abazov *et al.*, *Phys. Rev. Lett.* **103** (2009) 092001, [0903.0850](#).
8. CDF Collaboration, T. Aaltonen *et al.*, *Phys. Rev. Lett.* **101** (2008) 252001, [0809.2581](#).
9. CDF Collaboration, T. Aaltonen *et al.*, *Phys. Rev. Lett.* **103** (2009) 092002, [0903.0885](#).
10. S. Frixione, E. Laenen, P. Motylinski, and B. R. Webber, *JHEP* **03** (2006) 092, [hep-ph/0512250](#).
11. E. E. Boos, V. E. Bunichev, L. V. Dudko, V. I. Savrin, and A. V. Sherstnev, *Phys. Atom. Nucl.* **69** (2006) 1317–1329.
12. M. Beccaria, G. Macorini, F. M. Renard, and C. Verzegnassi, *Phys. Rev.* **D74** (2006) 013008, [hep-ph/0605108](#).
13. M. Beccaria *et al.*, *Eur. Phys. J.* **C53** (2008) 257–265, [0705.3101](#).
14. M. Beccaria *et al.*, *Phys. Rev.* **D77** (2008) 113018, [0802.1994](#).
15. E. Mirabella, *Nuovo Cim.* **123B** (2008) 1111–1117, [0811.2051](#).
16. N. Kidonakis, *Phys. Rev.* **D75** (2007) 071501, [hep-ph/0701080](#).
17. D. Bardin, S. Bondarenko, L. Kalinovskaya, G. Nanava, and L. Rumyantsev, *Eur. Phys. J.* **C52** (2007) 83–92, [hep-ph/0702115](#).
18. D. Bardin, L. Kalinovskaya, V. Kolesnikov, and W. von Schlippe, [0912.3893](#).
19. A. Pukhov *et al.*, [hep-ph/9908288](#).
20. A. Arbuzov *et al.*, *Eur. Phys. J.* **C46** (2006) 407–412, [hep-ph/0506110](#).
21. A. Arbuzov *et al.*, *Eur. Phys. J.* **C54** (2008) 451–460, [0711.0625](#).
22. A. Andonov *et al.*, *Comput. Phys. Commun.* **181** (2010) 305–312, [0812.4207](#).
23. A. Andonov *et al.*, *Phys. Part. Nucl. Lett.* **4** (2007) 451–460.